Do Hydroxyl Radical−Water Clusters, $OH(H_2O)_n$, $n = 1-5$, Exist in the Atmosphere?

Marco A. Allodi, Meghan E. Dunn, Jovan Livada, Karl N. Kirschner,* and George C. Shields*

Department of Chemistry, Hamilton College, 198 College Hill Road, Clinton, New York 13323

Received: July 14, 2006; In Final Form: September 27, 2006

It has been speculated that the presence of $OH(H_2O)_n$ clusters in the troposphere could have significant effects on the solar absorption balance and the reactivity of the hydroxyl radical. We have used the G3 and G3B3 model chemistries to model the structures and predict the frequencies of hydroxyl radical/water clusters containing one to five water molecules. The reaction between hydroxyl radical clusters and methane was examined as a function of water cluster size to gain an understanding of how cluster size affects the hydroxyl radical reactivity.

Introduction

The hydroxyl radical is the most important reactive species in the troposphere. Described as the atmospheric "vacuum cleaner," the hydroxyl radical is responsible for many of the reactions that remove volatile organic compounds (VOCs) from the air.[1] The hydroxyl radical has a short lifetime in the atmosphere and is regenerated constantly. It has a global average concentration of 10^6 molecules·cm^{-3} during the daylight hours, dropping at night once photodissociation pathways that generate OH cease.[1] Because the hydroxyl radical acts as a major sink for many VOCs, its concentration influences the balance of many atmospheric species. For example, this radical oxidizes approximately 83% of annual methane emissions, supporting the fact that the hydroxyl radical is one of the most important processors of greenhouse gases. Methane concentration is increasing in the atmosphere because anthropogenic sources are more than double natural methane sources, and sources outnumber sinks by 35−40 Tg·yr^{-1}.[1]

Because it is known to form singly hydrated complexes,[2,3] the role of the $OH(H_2O)$ dimer and higher order clusters has been speculated to have an effect on atmospheric chemistry. The formation of hydrogen bonds is known to affect the spectral features and reactivity of the constituent monomers.[4] Cluster formation results in spectral peak broadening, peak shifts, and the addition of intermolecular vibrational modes that occur below 1000 cm^{-1}. The $OH(H_2O)$ dimer, recently observed by rotational spectroscopy,[2,3] is proposed as an intermediate in the interconversion of OH and H_2O,[5] and has been predicted to be a stronger oxidant than free OH.[6] The presence of $OH(H_2O)_n$ clusters could have an effect on the solar absorption balance, resulting from the presence of new absorption bands ($<$1000 cm^{-1}) added to the atmospheric spectrum. Additionally, the larger dipole moment of the complex enhances the intensity of absorption.[7] In a recent review article, Schrems and co-workers argue that both the hydroxyl radical's solar absorption balance and reactivity could be greatly affected by complexation with water.[4] We have undertaken this study to better understand the role that $OH(H_2O)_n$ clusters could have on atmospheric absorption and reactivity with VOCs.

* Corresponding authors. E-mail: kkirschn@hamilton.edu; gshields@hamilton.edu.

Methods

The G3 model chemistry,[8] used previously to accurately model structures and energetics for gas-phase water clusters composed of 2−8 water molecules,[9−12] ion−water clusters,[13,14] and hydroperoxy radical−water complexes,[15] has been used to model the hydroxyl radical−water complexes. Clusters were built in SPARTAN,[16] optimized using the PM3 method,[17] and followed by HF/6-31G* self-consistent field optimizations.[18] These structures served as input for G3 calculations performed using Gaussian03 versions B.02 and C.02.[19] Harmonic frequency calculations were performed on all dimer, trimer, tetramer, pentamer, and hexamer structures using the HF/6-31G* method. These frequencies were scaled by 0.8929 to obtain reliable frequency estimates for the lowest energy structures because scaled HF/6-31G* frequencies have previously been shown to be in good agreement with MP2 anharmonic and experimental values for water clusters.[20] To understand the effects of clusters on reactivity, a simple reaction between hydroxyl radical clusters and methane was examined. Reactants, transition states, and products were calculated using the G3B3 method[21] because only one geometry optimization is required with this model chemistry. In addition to the model chemistry calculations, the BHandHLYP DFT functional was used with the 6-311G** and aug-cc-pVTZ basis sets to calculate geometries and harmonic frequencies for the methane and OH radical reaction pathway. A set of single self-consistent field calculations at the CCSD(T)/aug-cc-pVTZ level were made on the BHandHLYP/aug-cc-pVTZ geometries. Kinetic rate constants were obtained using TheRate on-line program[22] using simple transition-state theory with and without Eckart tunneling.[18,23,24]

Results

The free-energy minima at 298 K for the dimer, trimer, tetramer, pentamer, and hexamer are presented in Figure 1. The relevant O−H bond lengths and hydrogen bond lengths, angles, and other geometric parameters can be found in the Supporting Information. In addition, the remaining local minima for $OH(H_2O)_n$ $n = 2-5$ clusters can be found in the Supporting Information. Table 1 contains the G3 energetics in kcal·mol^{-1} for the association of cyclic water clusters with a hydroxyl radical and for the association of hydroxyl radical−water clusters with one additional water molecule. Our reported energetics

10.1021/jp064468l CCC: $33.50
Published on Web 11/18/2006

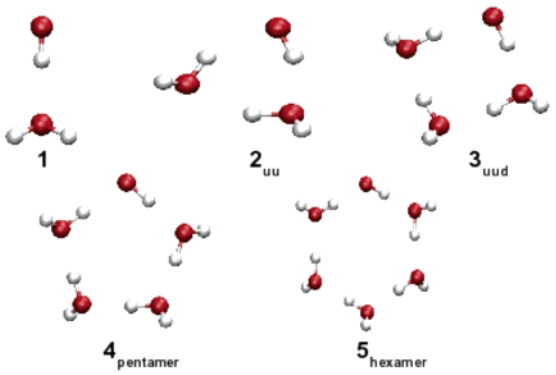

Figure 1. G3 free-energy minima at 298 K for $OH(H_2O)_n$ clusters, $n = 1-5$.

include the electronic energies of binding corrected for zero-point energy (ΔE_0), the same energies including thermal corrections ($\Delta E°_{298}$), and the enthalpies ($\Delta H°_{298}$) and Gibbs free energies ($\Delta G°_{298}$) at 298 K. Reaction i of Table 1 gives the association energetics for the formation of a hydroxyl radical−water cluster from a pure water cluster and free hydroxyl radical. Reaction ii of Table 1 gives the energetics for the sequential addition of water molecules to hydroxyl radical−water clusters.

The equilibrium constants for a standard state of 1 M (K_c), molarity (M), and the number of clusters/cm^3 predicted to be present in the lower troposphere on a humid day are presented in Table 2. These values are based on the Gibbs free energy for the association of the most stable $OH(H_2O)_{n-1}$ structure with each successive water (Table 1, reaction ii). Table 3 contains the results for the DFT calculations and for the CCSD(T) calculations for the reaction of OH and CH_4, from starting reactants to final products, including pre-reactive and post-reactive complexes, as well as the transition state for the reaction. Figure 2 illustrates the two-dimensional slice of the potential energy surface for this reaction using the data in Table 3. Table 4 contains ΔE_0, $\Delta E°_{298}$, $\Delta H°_{298}$, and $\Delta G°_{298}$ obtained using the G3B3 method for the reaction of methane with the OH radical, and the low energy C_{2v} dimer, cyclic trimer, cyclic tetramer, cyclic pentamer, and cyclic hexamer. This table also contains the G3B3 free energy of activation, $\Delta G°_{298}{}^{\ddagger}$, for the abstraction of a hydrogen from methane by the hydroxyl radical and by $OH(H_2O)_n$ clusters and rate constants. Table 5 contains scaled frequency data for the $OH(H_2O)$ dimer and $OH(H_2O)_2$ cyclic trimer.

Discussion

In the $OH(H_2O)$ dimer global minimum, OH is the hydrogen-bond donor.[2,3,25−34] The electronic state in the G3 structure has the radical electron in the in-plane $^2A'$ configuration, which is recognized as the global minimum for $OH(H_2O)$.[2,3,28,33,34] A second electronic state is close by, with the radical electron in the out-of-plane orbital, which corresponds to the higher energy $^2A''$ state.[26,28,32−34] The excited state lies ~200 cm^{-1} above the ground state.[2] The hydrogen-bond length for the ground state of 1.912 Å compares well with the microwave values of 1.952 Å[2] and 1.945 Å.[3] The transition state for the $OH(H_2O)$- - -H- - - CH_3 structure is also in the $^2A'$ electronic state, and the transition-state structure clearly shows that the radical electron that is in-plane is forming the bond with the hydrogen that is being abstracted from methane (Supporting Information).

The low-energy structures for the $OH(H_2O)_n$ trimer, tetramer, pentamer, and hexamer clusters at 298 K are cyclic, which are similar to the analogous pure water clusters.[10,12] A previous study by Hamad, Lago, and Mejías presents structures for the dimer through hexamer using the UMP2, BLYP, and BHLYP methods.[29] They found similar structures for MP2 energy minima for the dimer, trimer, and tetramer but different energy minima for the pentamer and hexamer. Mejías and co-workers' calculations using the BHLYP method reveal similar energy minima for all cluster sizes except the pentamer.[29] Cabral do Couto and co-workers used microsolvation modeling and statistical mechanics simulations to obtain $OH(H_2O)_n$ structures where $n = 1-6$.[31] Using the MPW1PW91/aug-cc-pVDZ method, they find low-energy structures that are similar to Mejías and co-workers' findings. For the trimer through hexamer, the low-energy structure is cyclic, with the free hydrogen on the water molecules alternating in an up (u), down (d) orientation. Conversely, Mejías finds the cyclic trimer to have water molecules with an up, up (u,u) orientation and the cyclic tetramer to have an up, down, down (u,d,d) orientation. Schenter and co-workers have used CCSD(T)/aug-cc-pVTZ potential scans of the $OH(H_2O)$ potential energy surface to devise an interaction potential for the ground and excited states of the OH radical−H_2O system.[7] Their interaction potential predicts cyclic structures as the lowest energy conformers for the trimer through pentamer, and the cage structure as the most stable hexamer.[7]

By our G3 calculations, the ΔE energy minima at 0 K are the ud cyclic trimer, udu cyclic tetramer, cyclic pentamer, and cage hexamer (Table 1). This agrees with previous MPW1PW91 DFT work.[31] The same structures are found as minima after adding thermal energy to obtain $\Delta E°_{298}$, with the exception of the hexamer, for which the prism is now the lowest energy structure. Gibbs free-energy calculations at 298 K reveal the most stable configurations at that temperature. Formation of the uu cyclic trimer, uud cyclic tetramer, cyclic pentamer, and cyclic hexamer have the lowest $\Delta G°$ values at 298 K. These structures, with the exception of the cyclic pentamer, are all different from the lowest energy structures determined from $\Delta E°$. This is a common occurrence with water clusters because the zero-point corrected energies yields the right order for the free-energy surface for these clusters in a cold (5−20 K) molecular beam, while raising the temperature reorders the free-energy profile.[11,12]

Hydrogen bond lengths shorten as the cluster size increases with the longest bond length for the OH to OH_2 hydrogen bond (Supporting Information). The OH to OH_2 hydrogen bond length is longest for the dimer at 1.9 Å, shortens to 1.8 Å for the trimer, 1.73 Å for the tetramer, 1.71 Å for the pentamer, and 1.70 Å for the hexamer. The HOH to OH hydrogen bond also shortens as cluster size increases. This suggests that the OH/water electron network strengthens with additional waters. The same trend of bond lengths can be seen in pure water clusters.[10] As cluster size increases for $OH(H_2O)_n$, $n = 2-5$, the hydrogen bond angle approaches 180°. The $OH(H_2O)$ dimer has a hydrogen bond angle of 173.5°, which compresses in the more constrained trimer, then increases to nearly 180° in the cyclic pentamer and hexamer. Brauer et al. have reported that the spin dipolar constants of the dimer increase by about 33% upon complexation while the Fermi contact term changes from −73.25 MHz in free OH to −155.3 MHz in the complex.[2] Although complicated to interpret for a multielectron effect, they state unequivocally that the large change in the OH magnetic hyperfine constants upon complexation leads to a substantial change in the electron distribution of the radical upon complexation.[2] Similarly, Ohshima and co-workers have concluded from their microwave results that electron density is transferred from the water to the OH radical upon formation of the hydrogen-bonded complex.[3] Our results lead us to suggest that,

TABLE 1: G3 Energetics in kcal·mol^{-1} for the (i) Association of Cyclic Water Clusters with Hydroxyl Radical, and (ii) Incremental Association of Hydroxyl Radical−Water Clusters with an Additional Water Molecule

(i) $(H_2O)_n + OH \rightarrow HO(H_2O)_n$

(ii) $HO(H_2O)_{n-1} + H_2O \rightarrow HO(H_2O)_n$

n	ΔE_0		ΔE°_{298}		ΔH°_{298}		ΔG°_{298}	
	i	ii	i	ii	i	ii	i	ii
1	−3.97	−3.97	−3.90	−3.90	−4.49	−4.49	1.14	1.14
2_{ud}	−6.93	−6.16	−7.58	−6.59	−8.17	−7.18	1.56	2.36
2_{uu}	−6.83	−6.05	−7.32	−6.33	−7.91	−6.92	1.37	2.17
3_{pud}	−4.84	−5.17	−4.51	−4.83	−5.10	−5.42	1.41	1.74
3_{uud}	−8.79	−9.12	−8.64	−8.97	−9.24	−9.56	−1.74	−1.38
3_{udu}	−9.03	−9.35	−9.04	−9.36	−9.63	−9.95	−1.48	−1.14
4_{S4+OH}	−5.39	−6.20	−5.32	−6.18	−5.91	−6.77	2.18	2.39
4_{D2d}	−4.87	−5.68	−4.74	−5.60	−5.33	−6.19	2.48	2.70
$4_{udu+H2O}$	−2.54	−3.36	−2.03	−2.90	−2.62	−3.49	4.10	4.32
$4_{pentamer}$	−5.39	−7.57	−5.32	−7.29	−7.02	−7.88	−0.23	−0.01
$5_{hexamer}$	−5.84	−6.32	−5.57	−5.97	−6.16	−6.56	−3.30	0.83
5_{book}	−4.56	−5.04	−4.56	−4.97	−5.16	−5.56	−0.55	3.58
$5_{pentamer+OH}$	−4.29	−4.77	−4.34	−4.75	−4.94	−5.34	−0.60	3.53
5_{cage}	−6.27	−6.75	−6.81	−7.21	−7.40	−7.80	−0.55	3.58
5_{prism}	−5.87	−6.34	−6.33	−6.73	−6.92	−7.32	−0.13	3.99

TABLE 2: Gibbs Free Energies (Standard State of 1 M) in kcal·mol^{-1}, Equilibrium Constants (Standard State of 1 M), Molarity (M), and Number of Hydroxyl Radical Clusters per Cubic Centimeter (N) Predicted to be Present in the Lower Troposphere when the Water Concentration is 0.001544 M, and the OH Concentration is 1.66058×10^{-14} M, at 298 K

reaction	ΔG°_{298}	K_c	M	N
$OH + H_2O \rightarrow HO(H_2O)$	1.14	3.56	9.1×10^{-17}	5.5×10^{4}
$HO(H_2O) + H_2O \rightarrow HO(H_2O)_2$	2.17	0.631	6.4×10^{-20}	4×10^{1}
$HO(H_2O)_2 + H_2O \rightarrow HO(H_2O)_3$	−1.38	251	2.4×10^{-20}	1.4×10^{1}
$HO(H_2O)_3 + H_2O \rightarrow HO(H_2O)_4$	−0.0144	25.1	9.1×10^{-22}	5.5×10^{-1}
$HO(H_2O)_4 + H_2O \rightarrow HO(H_2O)_5$	0.828	6.05	8.5×10^{-24}	5×10^{-3}

TABLE 3: Change in Electronic Energy, Gibbs Free Energy, Enthalpy, Entropy, and Activation Energy for the Formation of CH_3 and H_2O from OH and CH_4[a]

	ΔE_0	ΔH°_{298}	ΔG°_{298}	ΔS°_{298}	E_a[b]
		BHandHLYP/aug-cc-pVTZ[c]			
reactants → pre-reactive complex	0.20	0.72	1.43	−7.85	
reactants → transition state	8.36	7.37	13.30	−20.71	8.56
reactants → post-reactive complex	−10.04	−9.44	−7.50	−8.34	
reactants → product	−9.83	−9.42	−12.23	9.51	
		CCSD(T)/aug-cc-pVTZ[c]			
reactants → pre-reactive complex	−0.15	0.37	1.09	−2.39	
reactants → transition state	4.51	3.53	9.45	−19.87	4.72
reactants → post-reactive complex	−14.21	−13.61	−11.68	−6.50	
reactants → product	−13.46	−13.05	−15.86	9.43	
pre-reactive complex → transition state	4.66	3.16	8.36	−17.48	
transition state → post-reactive complex	−18.73	−17.14	−21.13	13.37	
post-reactive complex → product	0.75	0.56	−4.18	15.92	
		experimental data			
reactant → transition state[d]		3.89			5.08

[a] Interaction energy given in kcal·mol^{-1}, and the change in entropy given in cal·mol^{-1}·Kelvin^{-1}. ΔE_0 includes zero-point vibrational energy. [b] Activation energy determined using the equation $E_a = \Delta H^{\circ\ddagger}_{298} + 2RT$. [c] Single self-consistent field calculation performed on BhandHLYP/aug-cc-pVTZ optimized geometries. [d] Reference 42.

similar to pure water clusters, the cooperativity of hydrogen-bond formation distributes the partial atomic charge throughout the cluster. This effect for homodromic cyclic water clusters was first explained by Xantheas,[35] and can be seen in homodromic cyclic water structures for trimers, tetramers, pentamers, and octamers.[11,12] The cyclic structures that display cooperativity have their individual water dipoles building upon each other in the plane of the cycle, resulting in more negative charge on the oxygens and more positive charge on the hydrogens in cooperative complexes.[12] The partial atomic charges on OH, H_2O, and $OH(H_2O)$ derived from the electrostatic potential at the UMP2-(full)/6-31G* level reveal that the water hydrogens become more positive by 0.014 atomic charge in the complex, the hydroxyl hydrogen becomes more positive by 0.050 atomic charge, and the hydroxyl oxygen becomes more negative by 0.074 atomic charge.

The concentration of clusters in the atmosphere at 298 K is estimated in Table 2, for a water vapor concentration of 0.001544 M and a hydroxyl concentration of 1.66058×10^{-14} M. The equilibrium constant, K_c, (1 M standard state) is calculated from ΔG° (1 atm standard state) values from Table 1(ii). This table shows the incremental change in free energy for an existing $OH(H_2O)_n$ cluster upon incorporating another water molecule into the complex, and the abundances of specific clusters. The most abundant of the clusters, $OH(H_2O)$, is predicted to have a concentration on the order of 10^4 molecules·cm^{-3} on a warm humid day. The dimer concentration

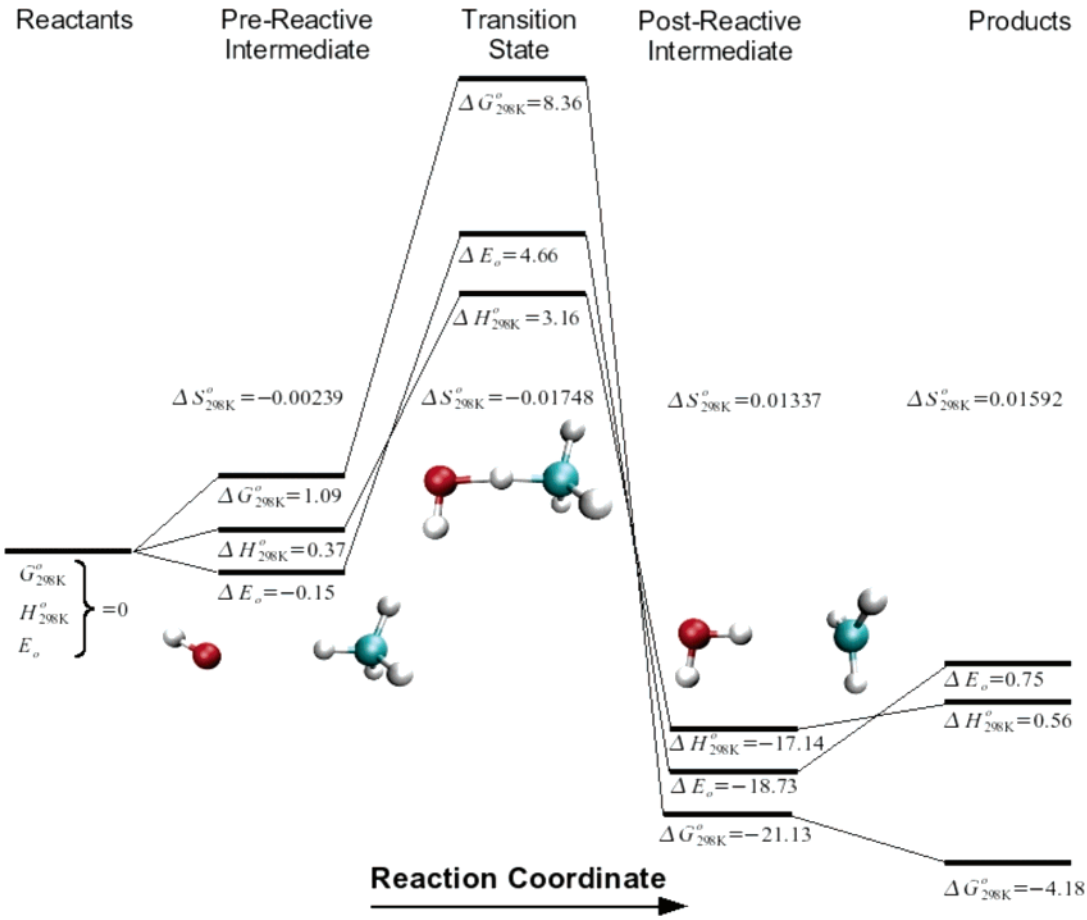

Figure 2. Two-dimensional view of the potential energy surface for the reaction of OH + CH_4 → H_2O + CH_3 using the CCSD(T)/aug-cc-pVTZ//BHandHLYP/aug-cc-pVTZ results. Energies in kcal·mol^{-1} and entropies in kcal·mol^{-1}·K^{-1}.

TABLE 4: G3B3 Change in Energy, Enthalpy, Gibbs Free Energy, and Activation Energy with Calculated Transition-State Theory Rate Constants at 298 K for the Formation of a $CH_3(H_2O)_{n+1}$ Cluster from $OH(H_2O)_n$ and CH_4[a]

	$CH_4 + OH(H_2O)_n \rightarrow CH_3+(H_2O)_{n+1}$						
n	ΔE_0	ΔE°_{298}	ΔH°_{298}	ΔG°_{298}	$\Delta G^{\circ\ddagger}_{298}$	k^b	k^c
0	−13.4	−14.5	−14.0	−12.5	9.7	3.9×10^{-14}	2.0×10^{-13}
1	−13.1	−13.7	−13.7	−8.2	13.7	2.4×10^{-16}	8.7×10^{-16}
2	−14.8	−15.8	−15.4	−9.1	10.6	3.0×10^{-15}	1.2×10^{-14}
3	−14.3	−15.4	−14.9	−8.2	10.5	1.3×10^{-15}	6.9×10^{-15}
4	−14.5	−15.4	−15.1	−7.4	12.7	8.9×10^{-17}	4.1×10^{-16}
5	−14.0	−14.9	−14.6	−7.3	11.7	3.5×10^{-16}	1.5×10^{-15}

[a] Interaction energies are reported in kcal·mol^{-1}, and the rate constants are reported with units of cm^3·molecule^{-1}·s^{-1}. [b] Rate constant determined without proton tunneling. [c] Rate constant determined with Eckart proton tunneling.

is on the same order of magnitude as the water hexamer, which would be difficult to detect in the troposphere.[9] However, this does not rule out the possibility that the $OH(H_2O)_n$ clusters could have an important role in atmospheric chemistry. This is an equilibrium calculation based on an initial population for the hydroxyl radical of 10^7 radicals/cm^3. If local conditions produced a 1000th-fold increase in the OH concentration, then the OH-(H_2O) cluster concentration would increase to 10^7 clusters·cm^{-3}. Measurement of OH concentrations are complicated,[36,37] and researchers are continually trying to improve modeling and experimental methods for accurate determination of this important radical.[38−42] There is evidence for substantial variation of the concentration of hydroxyl radicals over the past several decades.[41] Field measurements and modeling studies differ between observation and predictions of OH concentration in the atmosphere, and the importance of weak electronic absorption features in contributing to significant OH production has been demonstrated.[43] On the basis of the currently accepted values for the abundances of OH, and our thermodynamic results, we do not expect clusters of $OH(H_2O)_n$ to be abundant in the atmosphere.

To put the reactivity of $OH(H_2O)_n$ clusters in context, consider Table 3, which illustrates the reactivity of the clusters by displaying the values for removing a hydrogen from methane. The oxidation of methane by the hydroxyl radical is one of the two major sources of water in the stratosphere, the other being water injection from the troposphere.[44] Experimentally, the activation barrier (E_a) for the reaction

$$CH_4 + OH \rightleftharpoons CH_3 + H_2O$$

is 5.08 kcal·mol^{-1}, and when corrected for $2RT$ results in a $\Delta H^{\circ\ddagger}$ of 3.89 kcal·mol^{-1}.[45] The CCSD(T)/aug-cc-pVTZ method yields a $\Delta H^{\circ\ddagger}_{298}$ of 3.5 kcal·mol^{-1} and an E_a of 4.7 kcal·mol^{-1}, in agreement with the experimentally observed activation barrier. The G3B3 method is also in good agreement, producing values

TABLE 5: Vibrational Modes, Frequencies in cm^{-1}, and Relative IR Intensities for the OH(H_2O) Dimer and OH(H_2O)$_2$ Cyclic Trimer from HF/6-31G* Scaled Harmonic Frequencies[a]

mode	frequency	IR intensity
	OH(H_2O)	
ν_3	3738	m
ν_1	3636	w
O−H stretch	3517	s
ν_2	1624	m
out-of-plane ω	541	s
in-plane ω	395	s
heavy atom stretch	173	w
τ (H_2O), ω (OH)	135	w
ω (H_2O)	122	s
	OH(H_2O)$_2$	
ν_3 (D)	3717	m
ν_3 (A)	3711	m
ν_1 (D)	3596	m
ν_1 (A)	3563	s
OH stretch	3439	s
ν_2^c (AD)	1651	m
ν_2^{nc} (A/D)	1635	m
ω^c (ADOH)	767	m
ω^{nc} (AD/OH)	550	s
ω^{nc} (A/OH)	459	s
τ^{nc} (A/D)	407	s
ρ^c (AD), ω (OH)	336	m
ρ^{nc} (A/D)	257	m
heavy atom str (AOH)	202	w
distortion	170	w
ω (A, free H)	166	m
heavy atom str (DOH)	136	w
ω (AD, free H)	100	m

[a] The relative intensity for infrared absorption (IR) are characterized as weak (w; < 40 KM/mole), medium (m; 60−160 KM/mol), or strong (s; > 195 KM/mol), and the scale factor is 0.8929. Key to mode motion: c for concerted, nc for nonconcerted, ω for wag, ρ for rock, and τ for twist. The "plane" refers to the mirror symmetry plane of the dimer. For the trimer, D and A stand for the donor and acceptor waters, respectively.

for $\Delta H^\circ_{298}{}^{\ddagger}$ of 3.8 kcal·mol^{-1} and for $\Delta G^\circ_{298}{}^{\ddagger}$ of 9.7 kcal·mol^{-1}. A two-dimensional slice of the potential energy surface for this reaction is shown in Figure 2. This curve was generated by taking the energy at each point relative to the preceding point, considering the forward reaction above and is also reported in Table 3. The curve can be described by three different types of energies: zero-point vibrationally corrected electronic energy (ΔE_0), enthalpy (ΔH°_{298}), and Gibbs free energy (ΔG°_{298}). A pre-reactive and post-reactive intermediate are formed on the ΔE_0 surface, whereas only the post-reactive intermediate is seen on the ΔH°_{298} surface. Formation of the pre-reactive complex from the reactants has an entropic cost, as does formation of the transition-state structure from the pre-reactive complex. Formation of the post-reactive intermediate from the transition-state structure has a favorable entropy change, as does production of the final products from the post-reactive intermediate. At room temperature and with entropy taken into account, neither intermediate is a stationary point on the ΔG°_{298} surface. The free energy of activation at room temperature is the free energy for the transition from the reactants to the transition state, 1.09 + 8.36, or 9.45 kcal·mol (Figure 2). As the temperature is lowered toward zero Kelvin, the ΔH°_{298} and ΔG°_{298} surfaces converge to the ΔE_0 surface. At very low temperatures, as found in a molecular beam, it would be possible to observe both the pre- and post-intermediates of this reaction.

Given the expense of the CCSD(T) calculations, we found that the model chemistry G3B3 method was able to provide reasonable results at a lower cost, as seen in comparing Table 4 to Table 3. As shown in the table, the hydration of OH actually reduces the Gibbs free energy released by the reaction, as well as increasing the Gibbs activation energy. In general, water clusters reduce the oxidative ability of OH with respect to methane. Thus, it appears that any water clusters that form about the hydroxyl radical will reduce, not enhance, the rate of reaction of OH with organic species in the atmosphere. We attribute this effect to the enhanced stability of OH(H_2O)$_n$ clusters as the number of waters, *n*, increases. As each successive water is added to make the most stable cluster, the OH to OH_2 hydrogen bond strengthens, as does the OH/water electron network. This result contradicts an earlier conclusion based on semiempirical quantum mechanical calculations.[6] Karakus and Ozkan have shown that the difference in electronic energy between transition-state structures and reactants for the reaction of OH(H_2O) abstracting a hydrogen from alkanes decrease as the hydrocarbon chain is increased from one (methane) to three (propane).[46]

The experimental rate constant $CH_4 + OH \rightarrow CH_3 + H_2O$ has been determined by multiple research groups for temperature ranges from 1240 to 190 K.[47−52] The most recent experimental determination of the rate constant is $6.29 \pm 0.18 \times 10^{-15}$ to $6.8 \pm 0.14 \times 10^{-15}$ cm^3·molecule^{-1}·s^{-1} at 298 K.[53] A comprehensive review by Atkinson summarizes the methods and rate constants obtained from experiments from 1962 to 2002, and he recommends a value of 6.40×10^{-15} cm^3·molecule^{-1}·s^{-1}.[52] Using the G3B3 model chemistry results and TheRate on-line program, we determined rate constants for this reaction to be 3.9×10^{-14} cm^3·molecule^{-1}·s^{-1} and 2.0×10^{-13} cm^3·molecule^{-1}·s^{-1} when including tunneling in the rate constant calculation. Both of these values are approximately 10 and 100 times larger than the experimental value. In 1993, Melissas and Truhlar used MP2-SAC2 model chemistry results and interpolated canonical variational transition-state theory with tunneling and obtained rate constants at 298 K, $4.12-5.48 \times 10^{-15}$ cm^3·molecule^{-1}·s^{-1}, results that are remarkably close to today's accepted values.[23,54]

We can draw some conclusions from Table 4 if we consider that the error in the rate calculation is systematic and we only examine the relative rates as a function of hydration extent of the hydroxyl radical. Considering the tunneling-corrected rate constant, the hydration of the hydroxyl radical decreases the rate by 10- to 1000-fold, the slowest rate obtained being the hydration of the radical by a single water molecule. As discussed above, we predict that the OH(H_2O)$_n$ cluster will have an abundance of 5.5×10^4 molecules in the lower atmosphere, and a 1000-fold decrease in its reaction with methane.

The hydroxyl OH stretch of the dimer has been observed in an argon matrix at 11.5 K and assigned to bands at 3452 and 3428 cm^{-1}.[28] Later work that coupled these experiments with highly accurate anharmonic oscillator local-mode calculations revealed three bands, at 3452.2, 3428.0, and 3442.1 cm^{-1}. These three sites most likely stem from different sites within the matrix, and not from different structures, and their scaled model gives a single value of 3479.0 cm^{-1}.[33] Our gas-phase value is 3517 cm^{-1}, well within the perturbations induced by the argon matrix.[20] For spectroscopic detection of OH(H_2O)$_n$ clusters, we will focus on those vibrations that are unique and have strong intensities for the dimer and trimer because larger clusters are probably not abundant enough for detection. We have shown previously that HF/6-31G* scaled frequencies for water clusters have standard deviations of 20−25 cm^{-1} compared to experimental and to MP2 anharmonic frequencies.[20] According to the scaled HF/6-31G* frequencies, the hydroxyl radical has a vibration at 3569 cm^{-1}. The OH(H_2O) dimer has an OH stretch

red shifted from the OH monomer by 52 cm^{-1}, whereas the $OH(H_2O)_2$ trimer's OH stretch is red shifted from the dimer by 78 cm^{-1}. Because of this difference in frequencies, the trimer could possibly be identified by IR spectroscopy through the 3439 cm^{-1} OH stretch. An isolated dimer could be observed at its 3517 cm^{-1} OH stretch, but this vibration would most likely be overlapped by a ν_1 $(H_2O)_3$ vibration at 3519 cm^{-1} and a ν_1 $(H_2O)_4$ vibration at 3521 cm^{-1} unless the water concentration could be reduced significantly in the IR experiment.[20]

The intermolecular vibrational modes at 541 cm^{-1} (an out-of-plane wag), 395 cm^{-1} (in-plane wag), and 122 cm^{-1} (wag) are three possible targets for detecting $OH(H_2O)$. The ν_1 vibration of $OH(H_2O)_2$ at 3563 cm^{-1}, and intermolecular vibrational modes at 550, 459, and 407 cm^{-1} have strong IR intensities that could assist in the detection of $OH(H_2O)_2$. The 550 cm^{-1} vibration is a nonconcerted wag of the acceptor and donor waters wagging out-of-phase with the OH wagging motion. This $OH(H_2O)_2$ peak could potentially be overlapped if the water dimer (vibration at 553 cm^{-1}) or water pentamer (vibration at 449 cm^{-1}) were present under experimental conditions.[20] A similar overlap with the 407 cm^{-1} vibration of $OH(H_2O)_2$, a nonconcerted twist of the acceptor water and donor water, which would be hidden by an intermolecular mode of the water trimer. If such water clusters were present in the experimental setup, then the 459 cm^{-1} vibration of $OH(H_2O)_2$ (a nonconcerted wagging of the acceptor water and hydroxyl radical) is unique from other clusters, thus a good target for detection. Another possibility for observing these complexes is to probe electronic transitions. The electronic transition $^2\Sigma^+ \leftarrow {}^2\Pi$ occurs around 308 nm, and this transition is predicted to red shift by about 2500 cm^{-1} upon formation of the $OH(H_2O)$ complex.[34]

Conclusions

The G3 model chemistry has been used to determine the structures, energetics, and frequencies of $OH(H_2O)_n$ clusters. The lowest electronic energy structures agree with previous theoretical results. Free-energy calculations at 298 K reveal that the most likely structures to be observed at room temperature usually differ from the lowest temperature structures. The lowest free-energy structures display cooperativity of hydrogen bonding, maximizing the negative partial atomic charge on oxygens and the positive partial atomic charge on hydrogens involved in hydrogen bonding in these structures. The $OH(H_2O)$ geometry is in good agreement with the experimental microwave structure. Predicted abundances of the $OH(H_2O)_n$ clusters reveal that these clusters are not predicted to be abundant in the atmosphere. Calculation of free energies of activation for the abstraction of a hydrogen from methane predict that water impedes the ability of the hydroxyl radical to oxidize organic molecules, a result that is contrary to published hypotheses.

Acknowledgment. Acknowledgment is made to the donors of the Petroleum Research Fund, administered by the ACS, to Research Corporation, and to Hamilton College for support of this work. This project was supported in part by the U.S. Army Medical Research and Material Command's Breast Cancer Project grant W81XWH-05-1-0441, NIH grant 1R15CA115524-01, NSF grant CHE-0457275, and by NSF grants CHE-0116435 and CHE-0521063 as part of the MERCURY high-performance computer consortium (http://mercury.chem.hamilton.edu).

Supporting Information Available: Electronic energies, enthalpies, and free energies in Hartrees for all structures reported in this paper. Coordinates of all minima found with the G3 and G3B3 methods. Harmonic frequencies and IR and Raman intensities of the $OH(H_2O)$ and $OH(H_2O)_2$ clusters. This material is available free of charge via the Internet at http://pubs.acs.org.

References and Notes

(1) Seinfeld, J. H.; Pandis, S. N. *Atmospheric Chemistry and Physics: From Air Pollution to Climate Change*, 1st ed.; John Wiley & Sons: New York, 1998.

(2) Brauer, C. S.; Sedo, G.; Grumstrup, E. M.; Leopold, K. R.; Marshall, M. D.; Leung, H. O. *Chem. Phys. Lett.* **2005**, *401*, 420.

(3) Ohshima, Y.; Sato, K.; Sumiyoshi, Y.; Endo, Y. *J. Am. Chem. Soc.* **2005**, *127*, 1108.

(4) Sennikov, P. G.; Ignatov, S. K.; Schrems, O. *Chemphyschem* **2005**, *6*, 392.

(5) Aloisio, S.; Francisco, J. S. *Acc. Chem. Res.* **2000**, *33*, 825.

(6) Hobza, P.; Zahradnik, R. *J. Theor. Biol.* **1977**, *66*, 461.

(7) Du, S.; Francisco, J. S.; Schenter, G. K.; Iordanov, T. D.; Garrett, B. C.; Dupuis, M.; Li, J. *J. Chem. Phys.* **2006**, *124*, 224318.

(8) Curtiss, L. A.; Raghavachari, K.; Redfern, P. C.; Rassolov, V.; Pople, J. A. *J. Chem. Phys.* **1998**, *109*, 7764.

(9) Dunn, M. E.; Pokon, E. K.; Shields, G. C. *J. Am. Chem. Soc.* **2004**, *126*, 2647.

(10) Dunn, M. E.; Pokon, E. K.; Shields, G. C. *Int. J. Quantum Chem.* **2004**, *100*, 1065.

(11) Day, M. B.; Kirschner, K. N.; Shields, G. C. *Int. J. Quantum Chem.* **2005**, *102*, 565.

(12) Day, M. B.; Kirschner, K. N.; Shields, G. C. *J. Phys. Chem. A* **2005**, *109*, 6773.

(13) Pickard, F. C.; Pokon, E. K.; Liptak, M. D.; Shields, G. C. *J. Chem. Phys.* **2005**, *122*, 024302.

(14) Pickard, F. C.; Dunn, M. E.; Shields, G. C. *J. Phys. Chem. A* **2005**, *109*, 4905.

(15) Alongi, K. S.; Dibble, T. S.; Shields, G. C.; Kirschner, K. N. *J. Phys. Chem. A* **2006**, *110*, 3686.

(16) *SPARTAN*, 5.1.3 ed.; Wavefunction, Inc.: Irvine, CA 92612, 1998.

(17) Stewart, J. J. P. *J. Comput. Chem.* **1989**, *10*, 209.

(18) Cramer, C. J. *Essentials of Computational Chemistry: Theories and Models*, 2nd ed.; John Wiley & Sons: New York, 2004.

(19) Frisch, M. J.; Trucks, G. W.; Schlegel, H. B.; Scuseria, G. E.; Robb, M. A.; Cheeseman, J. R.; Montgomery, J. A., Jr.; Vreven, T.; Kudin, K. N.; Burant, J. C.; Millam, J. M.; Iyengar, S. S.; Tomasi, J.; Barone, V.; Mennucci, B.; Cossi, M.; Scalmani, G.; Rega, N.; Petersson, G. A.; Nakatsuji, H.; Hada, M.; Ehara, M.; Toyota, K.; Fukuda, R.; Hasegawa, J.; Ishida, M.; Nakajima, T.; Honda, Y.; Kitao, O.; Nakai, H.; Klene, M.; Li, X.; Knox, J. E.; Hratchian, H. P.; Cross, J. B.; Bakken, V.; Adamo, C.; Jaramillo, J.; Gomperts, R.; Stratmann, R. E.; Yazyev, O.; Austin, A. J.; Cammi, R.; Pomelli, C.; Ochterski, J. W.; Ayala, P. Y.; Morokuma, K.; Voth, G. A.; Salvador, P.; Dannenberg, J. J.; Zakrzewski, V. G.; Dapprich, S.; Daniels, A. D.; Strain, M. C.; Farkas, O.; Malick, D. K.; Rabuck, A. D.; Raghavachari, K.; Foresman, J. B.; Ortiz, J. V.; Cui, Q.; Baboul, A. G.; Clifford, S.; Cioslowski, J.; Stefanov, B. B.; Liu, G.; Liashenko, A.; Piskorz, P.; Komaromi, I.; Martin, R. L.; Fox, D. J.; Keith, T.; Al-Laham, M. A.; Peng, C. Y.; Nanayakkara, A.; Challacombe, M.; Gill, P. M. W.; Johnson, B.; Chen, W.; Wong, M. W.; Gonzalez, C.; Pople, J. A. *Gaussian 03*, revision C.02; Gaussian, Inc.: Wallingford, CT, 2004.

(20) Dunn, M. E.; Evans, T. M.; Kirschner, K. N.; Shields, G. C. *J. Phys. Chem. A* **2006**, *110*, 303.

(21) Baboul, A. G.; Curtiss, L. A.; Redfern, P. C.; Raghavachari, K. *J. Chem. Phys.* **1999**, *110*, 7650.

(22) Truong, T. N.; Nayak, M.; Huynh, H. H.; Cook, T.; Mahajan, P.; Tran, L. T.; Bharath, J.; Jain, S.; Pham, H. B.; Boonyasiriwat, C.; Nguyen, N.; Andersen, E.; Kim, Y.; Choe, S.; Choi, J.; Cheatham, T. E.; Facelli, J. C. *J. Chemical Inf. Model.* **2006**, *46*, 971.

(23) Truong, T. N.; Truhlar, D. G. *J. Chem. Phys.* **1990**, *93*, 1761.

(24) Truhlar, D. G.; Garrett, B. C.; Klippenstein, S. J. *J. Phys. Chem.* **1996**, *100*, 12771.

(25) Nanayakkara, A. A.; Balintkurti, G. G.; Williams, I. H. *J. Phys. Chem.* **1992**, *96*, 3662.

(26) Xie, Y. M.; Schaefer, H. F. *J. Chem. Phys.* **1993**, *98*, 8829.

(27) Wang, B. S.; Hou, H.; Gu, Y. S. *Chem. Phys. Lett.* **1999**, *303*, 96.

(28) Langford, V. S.; McKinley, A. J.; Quickenden, T. I. *J. Am. Chem. Soc.* **2000**, *122*, 12859.

(29) Hamad, S.; Lago, S.; Mejias, J. A. *J. Phys. Chem. A* **2002**, *106*, 9104.

(30) Zhou, Z. Y.; Qu, Y. H.; Fu, A. P.; Du, B. N.; He, F. X.; Gao, H. W. *Int. J. Quantum Chem.* **2002**, *89*, 550.

(31) do Couto, P. C.; Guedes, R. C.; Cabral, B. J. C.; Simoes, J. A. M. *J. Chem. Phys.* **2003**, *119*, 7344.

(32) Engdahl, A.; Karlstrom, G.; Nelander, B. *J. Chem. Phys.* **2003**, *118*, 7797.
(33) Cooper, P. D.; Kjaergaard, H. G.; Langford, V. S.; McKinley, A. J.; Quickenden, T. I.; Schofield, D. P. *J. Am. Chem. Soc.* **2003**, *125*, 6048.
(34) Schofield, D. P.; Kjaergaard, H. G. *J. Chem. Phys.* **2004**, *120*, 6930.
(35) Xantheas, S. S. *NATO ASI Ser., Ser. C* **2000**, *561*, 119.
(36) Heard, D. E.; Pilling, M. J. *Chem. Rev.* **2003**, *103*, 5163.
(37) Heard, D. E. *Annu. Rev. Phys. Chem.* **2006**, *57*, 191.
(38) Smith, S. C.; Lee, J. D.; Bloss, W. J.; Johnson, G. P.; Ingham, T.; Heard, D. E. *Atmos. Chem. Phys.* **2006**, *6*, 1435.
(39) Krol, M.; van Leeuwen, P. J.; Lelieveld, J. *J. Geophys. Res., [Atmos.]* **1998**, *103*, 10697.
(40) Krol, M.; van Leeuwen, P. J.; Lelieveld, J. *J. Geophys. Res., [Atmos.]* **2001**, *106*, 23159.
(41) Prinn, R. G.; Huang, J.; Weiss, R. F.; Cunnold, D. M.; Fraser, P. J.; Simmonds, P. G.; McCulloch, A.; Harth, C.; Salameh, P.; O'Doherty, S.; Wang, R. H. J.; Porter, L.; Miller, B. R. *Science* **2001**, *292*, 1882.
(42) Prinn, R. G.; Huang, J. *J. Geophys. Res., [Atmos.]* **2001**, *106*, 23151.
(43) Matthews, J.; Sinha, A.; Francisco, J. S. *Proc. Natl. Acad. Sci. U.S.A.* **2005**, *102*, 7449.
(44) Remsberg, E. E.; Bhatt, P. P.; Russell, J. M. *J. Geophys. Res., [Atmos.]* **1996**, *101*, 6749.
(45) DeMore, W. B.; Sander, S. P.; Howard, C. J.; Ravishankara, A. R.; Goldern, D. M.; Kolb, C. E.; Hampson, R. F.; Kurylo, M. J.; Molina, M. J. *Chemical Kinetics and Photochemical Data for Use in Stratospheric Modeling*; NASA/Jet Propulsion Laboratory, 1997.
(46) Karakus, N.; Ozkan, R. *J. Mol. Struct.: THEOCHEM* **2005**, *724*, 39.
(47) Vaghjiani, G. L.; Ravishankara, A. R. *Nature (London)* **1991**, *350*, 406.
(48) Finlaysonpitts, B. J.; Ezell, M. J.; Jayaweera, T. M.; Berko, H. N.; Lai, C. C. *Geophys. Res. Lett.* **1992**, *19*, 1371.
(49) Saunders, S. M.; K. J., H.; Pilling, K. J.; Baulch, M. J.; Smurthwaite, P. I. *Optical Methods in Atmospheric Chemistry*; SPIE: Berlin, 1992; Vol. 1715.
(50) Dunlop, J. R.; Tully, F. P. *J. Phys. Chem.* **1993**, *97*, 11148.
(51) Gierczak, T.; Talukdar, R. K.; Herndon, S. C.; Vaghjiani, G. L.; Ravishankara, A. R. *J. Phys. Chem. A* **1997**, *101*, 3125.
(52) Atkinson, R. *Atmos. Chem. Phys.* **2003**, *3*, 2233.
(53) Bryukov, M. G.; Knyazev, V. D.; Lomnicki, S. M.; McFerrin, C. A.; Dellinger, B. *J. Phys. Chem. A* **2004**, *108*, 10464.
(54) Melissas, V. S.; Truhlar, D. G. *J. Chem. Phys.* **1993**, *99*, 1013.